Int. J. Electrochem. Sci., 15 **(2020)** 5609 – 5622, doi: 10.20964/2020.06.07

International Journal of
ELECTROCHEMICAL
SCIENCE
www.electrochemsci.org

Effects of Side-Chain Polyether Additive on Zinc Electrodeposition from Ammoniacal Solution

Shenghai Yang[1], *Hua Liao*[1], *Zhimei Xia*[2,3*], *Yongming Chen*[1], *Duoqiang Zhao*[1],*Wenrong Lin*[1]

[1] School of Metallurgy and Environment, Central South University, Changsha 410083, China
[2] School of Metallurgy and Material Engineering, Hunan University of Technology, Zhuzhou, 412007, China
[3] Hunan Key Laboratory of Mineral Materials and Application, Central South University, Changsha 410083, China
[*]E-mail: zhimei_x@163.com

Received: 5 February 2020 / *Accepted:* 26 March 2020 / *Published:* 10 May 2020

A typical side-chain polyether, glycerol polyoxyethylene ether (GPE), was used as a single additive on zinc electrodeposition from ammoniacal solution. The electrochemical effects of GPE additive on zinc electrodeposition were investigated by means of cyclic voltammetry (CV), potentiodynamic polarization tests and chronoamperometry (CA). The morphology of zinc deposits on glassy carbon (GC) surface after zinc electrowinning was observed using SEM (scanning electron microscopy). The results indicated that the nucleation overpotential (NOP) was obviously increased up to 120 mV in addition of 1.5 g L^{-1} GPE in the electrolyte, and the hydrogen evolution reaction was significantly prevented in the presence of additive. The GPE additive has the effect to enhance cathodic polarization. In addition, the zinc electrodeposition process is greatly affected by agitation due to the diffusion control of Zn ion and the nucleation mechanism of zinc electrodeposition is independent of GPE. The more smooth, compact and fine-grained zinc deposits were obtained with 1.5 g L^{-1} GPE in the electrolyte.

Keywords: Zinc electrodeposition, Side-chain polyether, Ammoniacal solution, Electrochemical characterization, Deposit morphology

1. INTRODUCTION

As effective barrier and sacrificial coatings for ferrous substrates [1], electrodeposited zinc coatings are widely used in the field of corrosion resistant coatings and energy storage [2]. Traditionally, zinc electrodeposition is performed in sulphate baths, with halogen gas formed on the anode, which severely harming labourers' health, accelerating anodic corrosion and affecting the quality of zinc deposits. And the side reaction of hydrogen evolution on the cathode surface inhibits the deposition of Zn^{2+} and probably results in low current efficiencies (88–93%) and high energy consumption [3]. Zinc

redissolution can be occurred when other heavy metals are deposited on the cathode [4], and a process to decontaminate halides and exotic detrimental metals is required before electrodeposition. It is especially difficult and expensive to dispose of the electrolytes from secondary zinc materials, such as electric arc furnace dust and secondary zinc oxide from lead fuming furnaces, which contain high concentrations of chloride, fluoride and other noxious metals. Therefore it is necessary to find alternative electrolytes for zinc electrodeposition.

Electrodeposition of zinc from ammoniacal systems has attracted attention in recent years. Studies show that in ammonia ammonium chloride solution, leaching of zinc from low-grade oxide ore, electric arc furnace dust and secondary zinc oxide of lead fuming furnaces is feasible. In the leaching process, impurity elements such as iron, silicon, aluminium, and fluorine are mostly remained in the leaching residue other than into solution. High-purity zinc can be obtained by electrowinning from the leaching solution purified with zinc dust [5–7]. In recent years, many researchers have focused on the study of the role of various organic additives in electrodeposition of zinc and zinc alloys. During the electrodeposition of zinc, the additives added to the electrolytes are of great importance for modifying nucleation and crystal growth as well as changing the morphology of the zinc coatings [8–10]. In particular, the deposition rate of zinc is affected by organic substances adsorbed on the electrode [11]. A smooth, bright and compact zinc electrodeposit with high current efficiency and low energy consumption can be obtained by adding suitable additives [12]. It has been shown that the addition of polyethylene glycol (PEG) to the electrolyte can suppress the hydrogen evolution reaction (HER) and dendritic growth by adsorption of additive molecules on the deposit surface, which helps to achieve smooth and compact zinc and zinc alloy layers [13,14]. Gomes et al. indicated that the preferred orientation of Zn deposits obtained from solution containing anionic surfactant SDS was (101) and (102). The crystallographic orientation changes because the metal surface energy is modified by the adsorption of organic molecules [15].

Besides, Xia et al. concluded that the properties of the zinc–yttria-stabilized zirconia composite coatings were improved by adding gelatine to the solution [16]. Kavitha et al. reported that the zinc morphology was changed substantially and finer zinc grains were obtained in the presence of carbonyl compounds [17]. As reported by Sorour et al. the surface roughness of deposited zinc was improved effectively with the addition of 1-ethyl-3-methylimidazolium methane sulphate ([EMIM]MSO_3) and 1-butyl-3 methylimidazolium bromide ([BMIM]Br) as inhibitors and levellers, respectively [18].

Previous work from our group indicated that, in the presence of additive GPE in the electrolyte, the smoothness and compactness of zinc coatings were obviously improved and the current efficiency was also increased up to 92.88% [19]. The nucleation mechanism and growth orientation of zinc electrodeposition in ammoniacal solutions in the presence of gelatin were studied and the results indicated that the orientation of (101) plane was favourable for zinc deposition. The higher the diffraction peak, the more obvious the growth of zinc crystals [20].

In our present work, a typical side-chain polyether, glycerol polyoxyethylene ether (GPE), was used as a single additive on Zn electrodeposition from ammonia ammonium chloride solution, namely, ammoniacal solution. No experiments for using this organic substance as an additive in metal electrodeposition processes have been reported in any literature. In this paper, the electrochemical effects of GPE additive on zinc electrodeposition in ammoniacal solution were investigated through cyclic

voltammetry (CV), potentiodynamic polarization tests and chronoamperometry (CA) measurements. In addition, the morphology of zinc deposits on glassy carbon cathode surface after zinc electrowinning was also studied using a high resolution field emission scanning electron microscopy (SEM).

2. EXPERIMENTAL

2.1. Materials

Side-chain polyether, the organic additive used in this work, is glycerol polyoxyethylene ether (GPE), which is polymerized from glycerol and ethylene oxide, and its structural formula is shown in Figure 1.

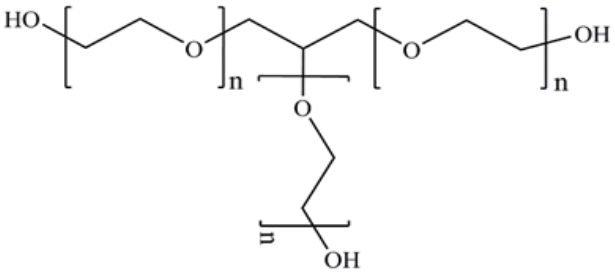

Figure 1. The structural formula of additive GPE

The simulated electrolyte containing 40 g L^{-1} Zn^{2+}, 5 mol L^{-1} NH_4Cl, and 1.8 mol L^{-1} NH_3 was prepared by dissolving appropriate amount of ZnO, NH_4Cl and $NH_3 \cdot H_2O$ (25 wt%) in deionized water, In the electrolyte, the zinc ions exist primarily in the form of zinc ammonia complexes, $Zn(NH_3)_4^{2+}$. And then the additive GPE with different concentrations from 0.50 g L^{-1} to 2.50 g L^{-1} was added into the electrolyte when Zn electrodeposition was carried out.

All chemical reagents were of analytical grade and purchased from Shanghai Jia Chen Chemistry Company of China.

2.2. Electrochemical measurements

All electrochemical characterisations were performed in a conventional three electrode cell using CHI760E Potentiostat/Galvanost (Shanghai CH Instrument Company, China) equipped with a computer running data acquisition software. A GC electrode with a geometric area of 0.07 cm^2, a saturated calomel electrode (SCE) and a platinum electrode (1.50 cm^2) were employed as the working electrode (WE), reference electrode and counter electrode (CE), respectively. All potentials shown in this paper were referred to reference electrode (SCE). All electrochemical experiments were conducted constantly at 40 ℃ without agitating.

Cyclic voltammetric measurements at different scanning rates without additive and at the scanning rate of 50 mV s^{-1} with various concentrations of GPE were recorded in the potential range from

the initial potential of –0.50 V and 0.50 V vs SCE respectively, to the final potential of –1.65 V vs SCE. The potentiodynamic polarization tests were carried out from −1.28 V to −1.52 V vs SCE with a scanning rate of 5 mV s^{-1}. To further investigate the kinetics behaviour of zinc electrodeposition in ammoniacal electrolytes containing 1.5 g L^{-1} GPE, an ATA-1 B zinc rotating disc electrode (RDE) with geometric area of 0.07 cm^2 was employed as working electrode. And the polarization experiments with zinc RDE were studied from –1.30 V to 1.95 V vs SCE at a sweep rate of 5 mV s^{-1}. Chronoamperometric tests were carried out within the potential range from –1.47 V to –1.49 V with various concentrations of GPE.

Before each measurement, nitrogen was bubbled for 0.5 h through 50 mL electrolytes to remove dissolved oxygen. The working electrode was polished with 3 μm abrasive paper, rinsed thoroughly with deionized water and ethanol, and finally dried with hot air for a few seconds.

Zinc electrowinning was conducted in a 2 L PVC electrolytic cell at current density 400 A m^{-2} for 8 h using graphite and titanium plate as anode (90 mm ×90 mm) and cathode (100 mm × 100 mm), respectively. After electrolysis, zinc deposits were washed by deionized water and ethanol, and then, dried in a vacuum condition. Finally, the surface morphology of the dried zinc films was performed by SEM using a JEOLJSM-5600LV microscope.

3. RESULTS AND DISCUSSION

3.1. Cyclic voltammetry

With the purpose to study the process of zinc electrodeposition, cyclic voltammetric experiments were performed. Figure 2(a) shows the cyclic voltammograms recorded for zinc electrodeposition from ammoniacal solution at different scanning rates without additive. The cyclic voltammetric scans on GC electrode were initiated at −0.50 V vs SCE in the cathodic direction and reversed at −1.65 V vs SCE in the anodic direction. The scanning rates were 10 mV s^{-1}, 20 mV s^{-1}, 30 mV s^{-1} and 40 mV s^{-1} respectively. Cathodic current can be barely observed before the potential reaches –1.28 V vs SCE, where corresponds to the beginning of the Zn ions reduction at the cathode, also known as nucleation potential. Then the current increased sharply, indicating that zinc deposited rapidly on cathodic surface.

In the cathodic voltammograms, two current peaks can be observed. The current peaks I at the potential of –1.50 V vs SCE correspond to the bulk zinc electrodeposition and the peak potentials shift to more negative values with the increasing of scanning rate. The current decreases after peak I due to the decreasing of zinc ions near the cathodic surface, which causes the appearing of current peaks II at about –1.60 V vs SCE corresponding to the hydrogen evolution reaction. The peak current of hydrogen evolution is much higher than that of zinc reduction with the scanning rate of 10 mV s^{-1}. And when the scanning speed is greater than 10 mV s^{-1}, the peak current of hydrogen evolution significantly decreases to less than the corresponding peak current of zinc reduction, indicating that the increasing scanning rate can inhibit the hydrogen evolution. In the anodic direction, one peak can be seen, due to the dissolution of zinc deposits formed previously.

It can be seen from Figure 2(a) that the peak I current density (j_d) increases with the scanning rate. According to the following Randles−Sevcik equation (Eq. 1), a linear relation between j_d and the

square root of scan rate ($v^{1/2}$) shown in Figure 2(b) indicates that the process of zinc deposition is controlled by mass transport [21,22]. Additionally, the peak I current density (j_d) value of 0.884 is larger than zero at $v^{1/2}$=0, which also comfirms that the nucleation process of zinc is controlled by mass transfer [23].The diffusion coefficient D is calculated as 2.59×10^{-9} cm^2 s^{-1} in the absence of GPE, which is much lower than that in traditional water based electrolyte [24] due to the formation of zinc ammonia complexes. Furthermore, there is no nucleation loop indicates that the Zn electrodeposition is not controlled by nucleation process. Namely, the zinc nuclei is much faster than the bulk growth. Zinc deposits obtained under such experimental conditions are likely to be randomly oriented with loose and irregular structure [25,26].

$$j_d = 0.4958zFCD^{1/2}v^{1/2}\left(\frac{\alpha zF}{RT}\right)^{1/2} \qquad \text{(Eq. 1)}$$

Where z is the number of electrons involved in the electrode process; α is the transfer coefficient, (equal to 0.392); and F is the Faraday constant (equal to 96485 C mol^{-1}). C is the concentration of Zn ions, M.

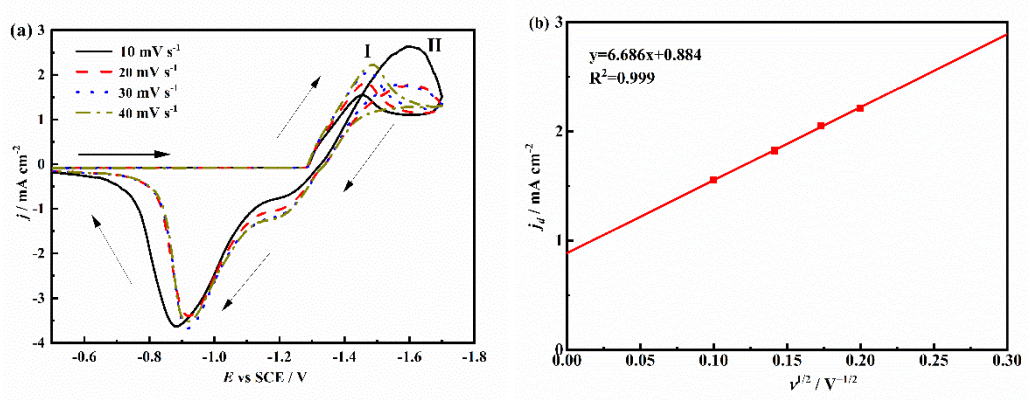

Figure 2. Cyclic voltammograms obtained on GC electrode with various scanning rates in additive-free electrolyte (a) and the linear relationship between peak I current density (j_d) with the square root of sweep rate ($v^{1/2}$) (b)

Figure 3 shows the cyclic voltammetric curves obtained on GC electrode with various concentrations of GPE in zinc ammoniacal solution at the scan rate of 50 mV s^{-1}. The enlarged views of peak currents and initial deposition potentials are shown in inserts (a) and (b), respectively. The cyclic scanning starts at point A and goes in the negative direction to points B and C, then reverses in positive direction towards point D and E, and again point A.

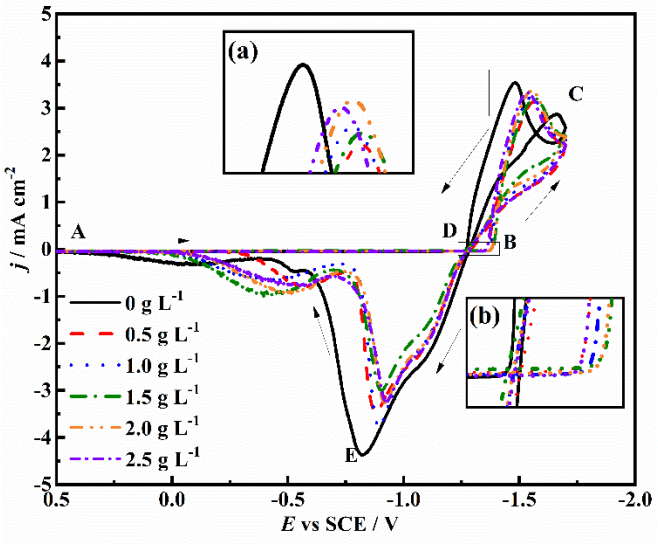

Figure 3. Cyclic voltammograms obtained on GC electrode with different concentrations of GPE in zinc ammoniacal solution. The scan rate is 50 mV s^{-1}

The cyclic voltammetric curves are significantly changed in the presence of additive, suggesting that both cathodic and anodic processes can be affected by the additive. Only one cathodic current peak can be observed corresponding to the reduction of Zn ions to metallic Zn, and no obvious hydrogen evolution current peaks are presented, which indicating that the additive GPE in the electrolyte can effectively inhibit the cathodic reduction of hydrogen ions. However, two peaks are obviously displayed in anodic scan, which may be related to the dissolution of crystalline Zn with (110) orientation plane at –0.87 V vs. SCE and the stripping of the crystal with random orientation at –0.51 V vs. SCE, this phenomenon was also observed in our previous studies [19], indicating that the effects of GPE on Zn electrodeposition in ammoniacal electrolyte were similar to those of gelatin.

The values of crossover potential (E_{CO}), the initiating potential for Zn^{2+} reduction (E), nucleation overpotential (*NOP*) and current density (j_d) as a function of GPE concentrations obtained from insets (a) and (b) are listed in Table 1. As shown in Table 1, a maximum j_d value appears without additive, which illustrates that the additive GPE has an inhibiting effect on zinc reduction process on GC electrode, this result is in accordance with that reported by Nayana et al [27]. The *NOP* is the potential difference between point D (crossover potential, E_{CO}) and B (the initiating potential for Zn^{2+} reduction on the cathode surface, E). *NOP* is used to illustrate the extent of cathodic polarization and high *NOP* values indicate strong polarization. It is also a characteristic parameter for identifying the optimum additive concentration during electrodeposition. The higher the *NOP*, the more compact and fine-grained zinc electrodeposited sheet [28]. It is observed from Table 1 that the *NOP* values are increased with appropriate amounts of GPE added, referring to an inhibition of zinc reduction on cathode. This is generally ascribed to the strong adsorption of additive layer on the GC electrode surface which increases the electrolyte viscosity and decreases the mass transfer. The *NOP* value obtains the maximum value 120 mV by adding 1.5 g L^{-1} of GPE to the electrolyte. However, the increase of GPE concentration up to 2.0 g L^{-1} and 2.5 g L^{-1} lowered the *NOP* values to 109 mV and 85 mV, respectively. It may be attributed that excessive adsorption of additive creates a barrier around the electrode surface and prevents the zinc

ions from discharging. Accordingly, a higher activation energy is required for the reduction of zinc ions with a higher nucleation rate and lower crystal growth rate.

Table 1 Values of E_{CO}, E, NOP and j_d on GC electrode as a function of GPE concentrations with scan rate of 50 mV s^{-1}

GPE concentration (g L^{-1})	E_{CO} (V)	E(V)	NOP(mV)	j_d(mA cm^{-2})
0	−1.296	−1.276	−20	3.53
0.5	−1.278	−1.364	86	3.14
1.0	−1.275	−1.374	99	3.23
1.5	−1.265	−1.385	120	3.19
2.0	−1.275	−1.384	109	3.32
2.5	−1.278	−1.363	85	3.31

3.2. Cathodic polarization

The potentiodynamic polarization is carried out to confirm the inhibition behavior and interaction kinetic of the GPE on the GC electrode surface. The Tafel curves for zinc electrodeposition from ammoniacal solution with different concentrations of GPE are depicted in Figure 4. It can be seen from the plots that the presence of GPE can induce significant changes in the polarization for zinc electrodeposition. The polarization curves are shifted to more negative potential with adding additive, which illustrating a suppressing effect on the reduction of zinc ion attributed to the adsorption of the GPE on the GC electrode surface. With the increasing of GPE concentration, the polarization becomes more obvious, which may be related to more adsorption of GPE on the cathode surface. It can block the active nucleation sites on the cathodic electrode surface and inhibit the zinc reduction process. The results are well consistent with the results obtained from cyclic voltammetry.

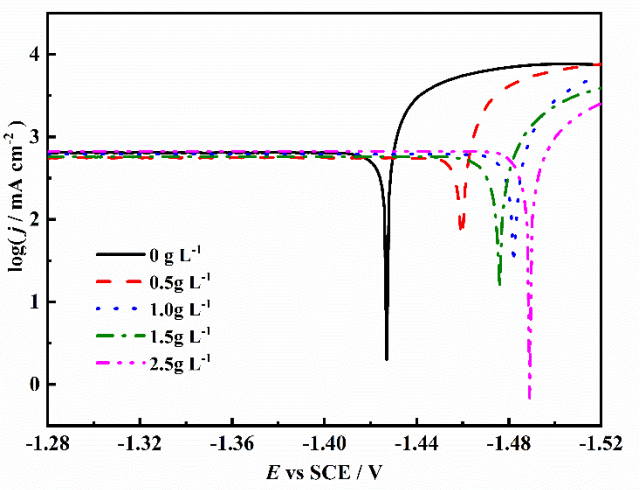

Figure 4. The Tafel curves on GC electrode with different concentrations of GPE in zinc ammoniacal solution. The scan rate was 5 mV s^{-1}

The kinetic parameters can be derived from Tafel curves by the following equation:

$\eta=a+b\log j$, $a=-\frac{RT}{\alpha zF}\ln j_0$, $b=2.303\frac{RT}{\alpha zF}$ (Eq. 2)

Where η is the overpotential, V; a is the overpotential where j=1 Am^{-2}; b is the Tafel slope; j_0 is the exchange current density, A m^{-2}, obtained by extrapolating the Tafel curve to the corresponding zero potential; α is the transfer coefficient.

According to Figure 4 and Eq. 2, the kinetic parameters, such as Tafel slopes (b), transfer coefficient (α) and exchange current densities (j_0), were calculated and listed in Table 2. The Tafel slope in the absence of additive is 63.33 mV $decade^{-1}$, which is close to that obtained from zinc sulfate electrolyte without additive(60 mV $decade^{-1}$) [29]; and it changes from 78.56 mV $decade^{-1}$ to 91.43 mV $decade^{-1}$ as the GPE concentration increases from 0.5 g L^{-1} to 2.5 g L^{-1}. With the increase of Tafel slope, the potential difference between anodic and cathodic region decreases, which resulting in a lower zinc deposition rate And the transfer coefficient changes slightly as the function of GPE concentration, indicating that additive GPE has no apparent influence on the transfer rate of Zn ions. The exchange current density attains a maximum value of 1.90×10^{-2} A cm^{-2} with no addition of GPE and gradually decreases to 1.33×10^{-2} A cm^{-2} as the concentration of GPE in ammoniacal electrolyte increases from 0.5 g L^{-1} to 2.5 g L^{-1}, and this also causes a lower zinc deposition rate. This is generally attributed to the active nucleation sites are blocked by the adsorption of additive on the cathode surface in the presence of additive in the solution. Apparently, the GPE concentration of 1.5 g L^{-1} results in optimal adsorption and a minimum value of j_0=1.32×10^{-2} A cm^{-2}. The smaller the exchange current density, the finer the zinc crystalline deposited on the substrate, as suggested by Morón et al [30]. Consequently, more compact and fine-grain zinc deposits can be obtained in the ammoniacal electrolyte with 1.5 g L^{-1} GPE.

Table 2. Values of b, α and j_0 on a stationary GC electrode with various concentrations of GPE in electrolyte

GPE concentration(g L^{-1})	b(mV $decade^{-1}$)	α	j_0($\times10^{-2}$ A cm^{-2})
0	63.33	0.39	1.90
0.5	78.56	0.35	1.53
1.0	89.72	0.34	1.34
1.5	91.43	0.32	1.32
2.5	90.32	0.33	1.33

To investigate the mass transport process of zinc electrodeposition in ammoniacal electrolyte containing 1.5 g L^{-1} GPE additive. A family of Tafel curves of Zn deposition obtained on zinc RDE at various speeds (200 rpm, 400 rpm, 600 rpm and 800 rpm) are presented in Figure 5. From Figure 5, it can be seen that the overpotentials are slightly shifted to positive direction when the rotating speed increases from 200 rpm to 800 rpm, indicating that the cathode polarization of zinc deposition is weakened by the rotating of electrode. Moreover, cathode polarization decreases with the increase of rotating rate, which can be inferred that the cathodic reaction is controlled by the diffusion. Namely, the higher the rotation speed, the faster the mass transfer rate of the electrolyte [31]. A constant current

density plateau is observed at the potential range of –1.65 V and −1.75 V vs. SCE, and the plateau region is narrowed with the increase of rotation speed. Leung et al interpreted this phenomenon as being a result of continuously supplied zinc ions to the electrode surface caused by the rotation of the electrode [32].

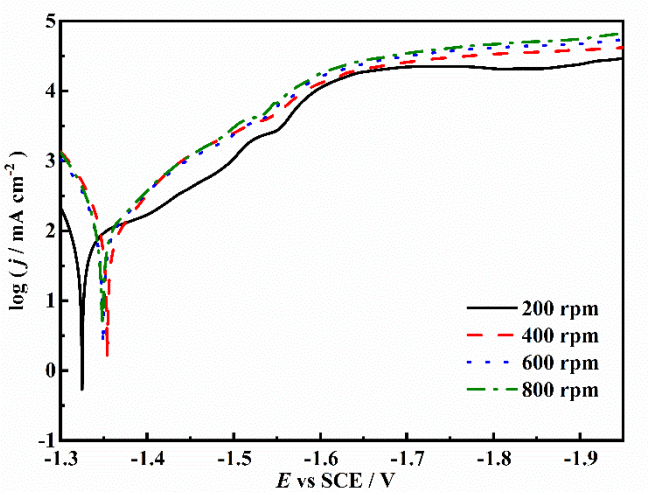

Figure 5. Tafel curves obtained on zinc RDE at different speeds with 1.5 g L^{-1} GPE in ammoniacal solution. The scan rate was 5 mV s^{-1}

A linear relationship between limited current density and the square root of the rotating rate deduced according to Levich equation (shown in Eq. 3) is presented in Figure 6.

$$j_d = 0.62zFD^{2/3}v^{-1/6}\omega^{1/2}c \qquad \text{(Eq. 3)}$$

Where D is the diffusion coefficient of the zinc ions, cm s^{-1}; v is the kinematic viscosity of the electrolyte, cm^2 s^{-1}; and ω is the rotating rate, s^{-1}.

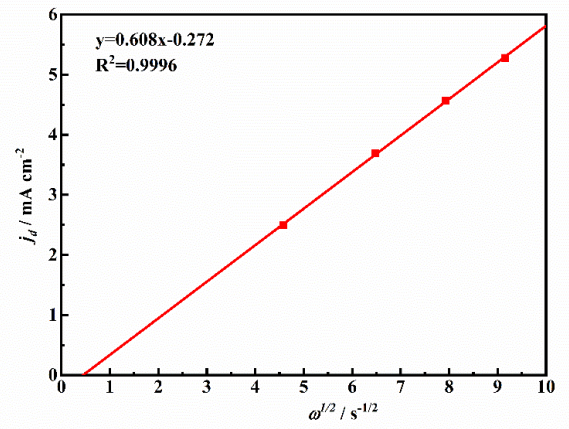

Figure 6. Dependence of limited current density (j_d) on the square root of rotating rate ($\omega^{1/2}$) on Zn RDE in ammoniacal solution at a scanning rate of 5 mV s^{-1}

As shown in Figure 6, the plot of j_d towards $\omega^{1/2}$ exhibits a straight line (correlation coefficient

of 0.9996), and the value of D is calculated from the slope of the straight line and Eq. 3 as 1.25×10^{-8} cm s^{-1}. In general, the electrolyte viscosity is increased with the adding of organic additive leading to a more difficult mass transport [33]. However, the diffusion coefficient (D) achieved with rotating disk electrode in present of GPE is even much larger than that with the stationary electrode with additive-free in electrolyte, indicating that agitation can significantly enhanced the mass transfer process, and it can also be inferred that the reduction process of zinc from ammoniacal solution is mainly controlled by diffusion rather than the electrochemical reaction.

3.3. Chronoamperometry

Chronoamperometry technique is employed to obtain the nucleation/growth mechanism of zinc electrodepositing on GC surface. Fig. 7 exhibits the potentiostatic current-time transients of Zn reduction process in ammoniacal solution with 1.5 g L^{-1} at various potentials (–1.47 V, –1.48 V,–1.49 V) at 40°C for 10 seconds. It can be seen from Figure 7 that all of these current–transient curves have a similar trend and exhibit typical three-dimensional diffusion–limited nucleation behaviour [34], corresponding to the results obtained from the polarization curves with RDE. The curves can be divided into two main steps. Initially, corresponding to double layer charging and the rapid nucleation of zinc, the cathode current density increases sharply to a maximum in a short time. Then, a decaying current density follows due to the consumption of the active species at the interface of GC electrode. It is significant to note that the j_d increases and the corresponding time (t_m) decreases when the step potential is shifted to a more negative value, which indicates that the rates of both nucleation and growth are increased. To determine the nucleation mechanism of zinc deposition, the experimental CA curves are preliminarily simulated with theoretical 3D instantaneous and progressive nucleation curves [35].

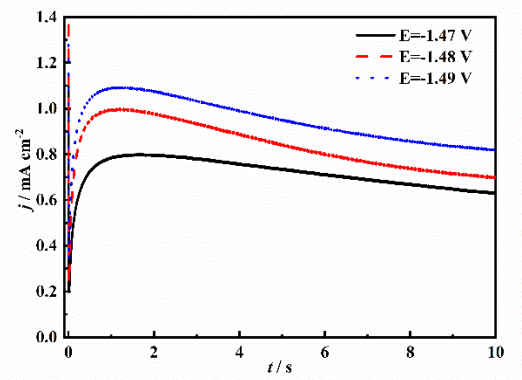

Figure 7. The potentiostatic current-time transients of Zn reduction process obtained on a GC electrode in ammoniacal solution with 1.5 g L^{-1} at different potentials

The equations of the theoretical 3D instantaneous and progressive models [36] are as follows.

3D instantaneous nucleation: $$\frac{j^2}{j_d^2}=\frac{1.9542}{t/t_m}\left\{1-\exp\left[-1.2564\left(\frac{t}{t_m}\right)\right]\right\}^2 \qquad \text{(Eq. 4)}$$

3D progressive nucleation: $$\frac{j^2}{j_d^2}=\frac{1.2254}{t/t_m}\left\{1-\exp\left[-2.3367\left(\frac{t}{t_m}\right)^2\right]\right\}^2 \qquad \text{(Eq. 5)}$$

The experimental chronoamperometric curves with different concentrations of GPE at –1.49 V (vs. SCE) were fitted, as shown in Figure.

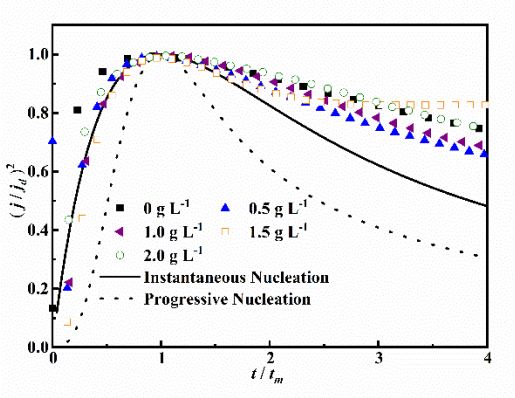

Figure 8. Comparison between the experimental and theoretical dimensionless curves with different GPE concentrations.

As shown in Figure 8, all the fitting curves follow the 3D instantaneous nucleation model at $t>t_m$, but the curves deviate from the model at $t<t_m$ both in the absence and presence of GPE, which may be indicated that the nucleation mechanism of Zn deposition were independent of GPE and that a secondary nucleation process existed. This nucleation mechanism is consistent with that of zinc electrodeposition from acid sulphate solution with salicylaldehyde and acetic acid as synergistic additive [23].

3.4. SEM characterization of zinc deposits

Surface morphology of the zinc deposits obtained from ammoniacal electrolyte with various concentrations of additive was examined using SEM and presented in Figure 9. The effects of additive GPE concentrations on the surface morphology of the deposited Zn were confirmed in terms of surface uniformity and morphology changes.

Figure 9(a) shows the zinc film deposited from the electrolyte without GPE. A dark grey porous zinc coating with loose and irregular structure can be found, a similar morphology of zinc deposition has already been shown in the relative literature [37,38], which may be ascribed to the drastic hydrogen evolution and zinc powders loosely covered on the cathode surface. Earlier studies have demonstrated that the loose and porous zinc coatings are easily formed in ammoniacal electrolytes [39]. The effective method to restrain the formation of mossy zinc deposits is to add organic additives into electrolyte solutions [18]. Figure 9(b-f) shows the SEM images of zinc deposits obtained with various concentrations of GPE in the electrolytes. It is clear that no loose zinc deposits have been formed. All zinc deposits exhibit bright metallic lustre and compact surface, indicating that the surface morphology of zinc deposits is effectively improved with adding GPE into electrolytes. Accordingly, it can be concluded that GPE as additive has a marked inhibition role on the formation of mossy zinc electrodeposits.

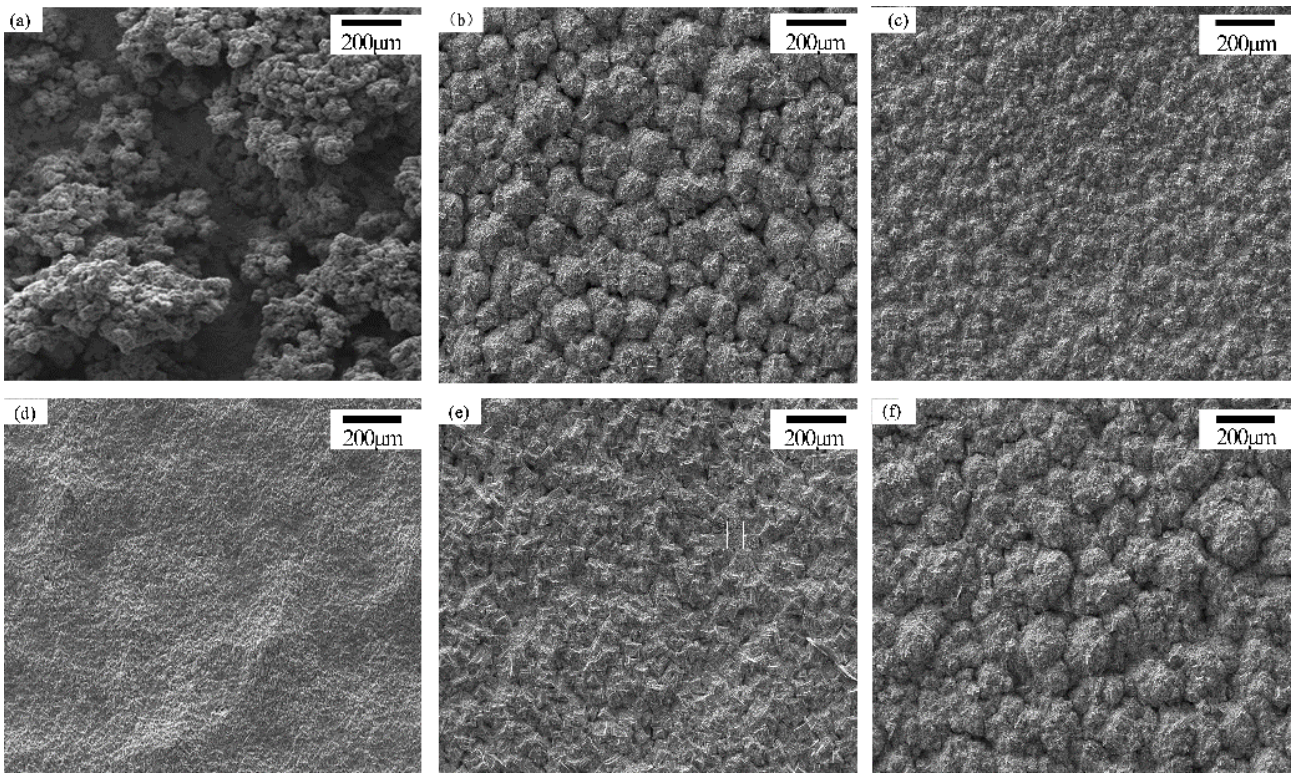

Figure 9. SEM images of the Zn deposits obtained with different concentrations of GPE in ammoniacal solution. (a)0 g L^{-1}; (b)0.5 g L^{-1}; (c)1.0 g L^{-1}; (d)1.5 g L^{-1}; (e)2.0 g L^{-1}; (f)2.5 g L^{-1}.

It is noteworthy that the more homogenous and smooth zinc deposits can be obtained with 1.5 g L^{-1} GPE compared to other concentrations of GPE (Figure 9d). These results are in agreement with previous electrochemical studies, indicating that the growth rate of Zn crystalline can be controlled by the GPE and 1.5 g L^{-1} of GPE has played the most effective role. It is possibly that the electrode surface cannot be covered completely when the concentration of the additive is less than 1.5 g L^{-1}, when the additive concentration is higher than 1.5 g L^{-1}, excessive GPE is adsorbed on the electrode, which results in less finer zinc deposits.

4. CONCLUSIONS

The effects of side-chain polyether, glycerol polyoxyethylene ether (GPE), on zinc elctrodeposition from zinc ammoniacal solution containing 40 g L^{-1} zinc ions have been investigated by measurements of cyclic voltammetry, potentiodynamic polarization curves, chronoamperometry and zinc electrowinning experiments.

The results showed that the nucleation overpotential was increased with additive in the electrolyte, and the addition of 1.5 g L^{-1} GPE caused the maximum increase of *NOP* value to 120 mV. The cathodic polarization was stimulated to inhibit the zinc reduction process. The hydrogen evolution reaction can be effectively suppressed by adding GPE in electrolyte, and more smooth, compact and fine-grained zinc deposits were obtained compared to that without additive. Additionally, the additive GPE had no apparent effect on the nucleation mechanism of zinc electrodeposition.

ACKNOWLEDGEMENTS
This work was supported financially by the National Natural Science Foundation of China (Grant No. 51704107), the National Basic Research Program of China (Grant No. 2014CB643404), the Hunan Provincial Natural Science Foundation of China (Grant No. 2018JJ3124), the Opening Project of Hunan Key Laboratory of Mineral Materials and Application (MMA201705) and the Fundamental Research Funds for the Central Universities of Central South University (2018zzts441).

References

1. P.A. Cantwell, P.P. Chung, H. Jiang, G.D. Wilcox and G.W. Crithlow, *Transactions of the IMF,* 86 (2008) 211.
2. H.Q. Liu, S. Szunerits, W.G. Xu and R. Boukherroub, *ACS Appl. Mater. Inter.,* 1 (2009) 1150.
3. B.C. Tripathy, S.C. Das, P. Singh, G.T. Hefter and V.N. Misra, *J. Electroanal. Chem.,* 565 (2004) 49.
4. A.R. Ault and E.J. Frazer, *J. Appl. Electrochem.,* 18 (1988) 583.
5. Z.M. Xia, M.T. Tang and S.H. Yang, *Can. Metall. Quart.,* 54 (2015) 439.
6. Y. Stefanov and I. Ivanov, *Hydrometallurgy*, 64 (2002) 193.
7. J. Wang, W. Xiong and B. Zhang, *Environ. Sci. Technol*., 37 (2014) 138.
8. H.F. Alesary, S. Cihangir, A.D. Ballantyne, R.C. Harris, D.P. Weston, A.P. Abbott and K.S. Ryder, *Electrochim. Acta,* 304 (2019) 118.
9. J.L. Ortiz-Aparicio, Y. Meas, G. Trejo, R. Ortega, T.W. Chapma and E. Chainet, *J. Appl. Electrochem.,* 43 (2013) 289.
10. H.F. Alesary, A.F. Khudhair, S.Y. Rfaish and H.K. Ismail, *Int. J. Electrochem. Sci.,* 14 (2019) 7116.
11. J. Nieszporek, D. Gugała-Fekner and K. Nieszporek, *Electroanalysis*, 31 (2019) 1141.
12. D.L. Piron, D. Mathieu and M. D'Amboise, *Can. J. Chem. Eng.,* 65 (1987) 685.
13. H. Kazimierczak, A. Hara, A. Bigos and P. Ozga, *Electrochim. Acta,* 202 (2016) 110.
14. A. Sharma, K. Das, H.J. Fecht and S. Das, *Appl. Surf. Sci.,* 314 (2014) 516.
15. A. Gomes and M.I. Dilva Pereira, *Electrochim. Acta,* 51 (2006) 1342.
16. X.L. Xia, I. Zhitomirsky and J. R. McDermid, *J. Mater Process Tech,* 209 (2009) 2632.
17. B. Kavitha, P. Santhosh, M. Renukadevi, A. Kalpana, P. Shakkthivel and T. Vasudevan, *Coat. Tech.,* 201 (2006) 3438.
18. N. Sorour, W. Zhang, G. Gabra, E. Ghali and G. Houlachi, *Hydrometallurgy,* 157 (2015) 261.
19. W.R. Lin, S.H. Yang, Y.W. Sun, Y.M. Chen, J. He and C.B. Tang, *The Chinese Journal of Nonferrous Metals,* 27 (2017) 399.
20. Z.M. Xia, S.H. Yang and M.T. Tang, *RSC Adv,* 5 (2015) 2663.
21. F.J. Barry and V.J. Cunnane, *J. Electroanal. Chem.,* 537 (2002) 151.
22. G. Trejo, H. Ruiz, R.O. Bores and Y. Meas, *J. Appl. Electrochem.,* 31 (2001) 685.
23. T. Minoru, A. Yoshihiro, Y. Yasutaka, B. Masaru, O. Shoko, O. Naoki, S. Takeyasu, Y. Masayuki and K. Kazuo, *The Electrochemical Society of Japan*, 82 (2014) 430.
24. F.J. Barry, V.J. Cunnane, *J. Electroanal. Chem.,* 151 (2002) 537.
25. H.F. Alesary, S. Cihangir, A.D. Ballantyne, R.C. Harris, D.P. Weston, A.P. Abbott and K.S. Ryder, *Electrochimi. Acta*, 304 (2016) 118.
26. S. Ibrahim, A. Bakkar, E. Ahmed .and A. Selim, *Electrochimi. Acta*, 191 (2016) 724.
27. K.O. Nayana and T.V. Venkatesha, *J. Electroanal. Chem.,* 663 (2011) 98.
28. P.T. Kissinger and W.R. Heineman, *J. Chem. Educ.,* 60 (1983) 702.
29. E. Guerra, *University of British Columbia*, 2003.
30. L.E. Morón, Y. Meas, R. Ortega-Borges, J.J. Perez-Bueno, H. Ruiz and G. Trejo, *Int. J. Electrochem.* Sci*.,* 4 (2009) 1735.
31. D.R. Gabe and D.J. Robinson, *Electrochim. Acta*, 17 (1972) 1121.

32. P.K. Leung, C. Ponce-de-León, C.T.J. Low and F.C. Walsh, *Electrochimi. Acta*, 18 (2011) 6536.
33. E. Barrado, J.A. Rodríguez and Y. Castrillejoa, *J. Electroanal. Chem.,* 804 (2017) 148.
34. J.C. Ballesteros, P. Dıaz-Arista, Y. Meas, R. Ortega and G. Trejo, *Electrochim. Acta*, 52 (2007) 3686
35. B.R. Scharifker and G. Hills, *Electrochim. Acta,* 28 (1983) 879.
36. B.R. Scharifker and J. Mostany, *J. Electroanal. Chem.,* 177 (1984) 13.
37. A.M. Alfantazi, D.B. Dreisinger, *Hydrometallurgy,* 69 (2003) 99.
38. A. Gomes, M.I. da Silva Pereira, *Electrochim. Acta,* 51 (2006) 1342.
39. W.M. Gu, C.Q. Liu, J. Tang, R.Y. Liu, H. Yang and J.G. Hu, *Hydrometallurgy,* 175 (2018) 43.